Published for SISSA by Springer

Received: August 8, 2023
Revised: October 11, 2023
Accepted: October 16, 2023
Published: October 30, 2023

Probing proton structure with $c\bar{c}$ correlations in ultraperipheral pA collisions

Barbara Linek,[a] **Agnieszka Łuszczak,**[b] **Marta Łuszczak,**[a] **Roman Pasechnik,**[c] **Wolfgang Schäfer**[d] **and Antoni Szczurek**[d]

[a] *University of Rzeszow, ul. Pigonia 1, Rzeszow PL-35-959, Poland*
[b] *Cracow University of Technology, Department of Physics, Kraków PL-30-084, Poland*
[c] *Department of Physics, Lund University, Lund SE-223 62, Sweden*
[d] *Institute of Nuclear Physics, Polish Academy of Sciences, ul. Radzikowskiego 152, Kraków PL-31-342, Poland*

E-mail: barbarali@dokt.ur.edu.pl, Agnieszka.Luszczak@pk.edu.pl, mluszczak@ur.edu.pl, Roman.Pasechnik@hep.lu.se, Wolfgang.Schafer@ifj.edu.pl, antoni.szczurek@ifj.edu.pl

Abstract: We study the exclusive diffractive $c\bar{c}$ photoproduction in ultraperipheral pA collisions. The formalism makes use of off-diagonal generalizations of the unintegrated gluon distribution, the so-called generalized transverse momentum dependent distributions (GTMDs). We present two different formulations. The first one is based directly on gluon GTMD parametrizations in momentum space. Another option is the calculation of the GTMD as a Fourier transform of the dipole-nucleon scattering amplitude $N(Y, \vec{r}_\perp, \vec{b}_\perp)$. The latter approach requires some extra regularization discussed in the paper. Different dipole amplitudes from the literature are used. Compared to previous calculations in the literature, we integrate over the full phase space and therefore cross sections for realistic conditions are obtained. We present distributions in rapidity of c or $\bar{c}$, transverse momentum of the $c\bar{c}$ pair, four-momentum transfer squared as well as the azimuthal correlation between a sum and a difference of the c and $\bar{c}$ transverse momenta. The azimuthal correlations are partially due to the so-called elliptic gluon Wigner distribution. Different models lead to different modulations in the azimuthal angle. The modulations are generally smaller than 5%. They depend on the range of transverse momentum selected for the calculation.

Keywords: Parton Distributions, Properties of Hadrons

ArXiv ePrint: 2308.00457

https://doi.org/10.1007/JHEP10(2023)179

Contents

1 Introduction

The diffractive production of high momentum particles, such as quark-antiquark dijets, serves as a probe of various aspects of the hadron structure [1]. For example, in the diffractive dissociation of photons or pions into dijets, the forward cross section at large jet transverse momenta maps out the unintegrated gluon distribution of the target [2, 3]. Recently, there has been much interest in a generalization of unintegrated (or transverse momentum dependent) parton distributions to a five-dimensional quasi-probability phase space distribution, known as the Wigner distribution [4, 5], which depends on both the transverse momentum and impact parameter of a parton in the proton or nucleus. When transformed fully to momentum space these are equivalent to the generalized transverse momentum distributions (GTMDs), see e.g. [6–8]. In particular, these distributions encode the dependence on the transverse momentum transfer $\vec{\Delta}_\perp$ to the target and, therefore, are of relevance for the description of the forward cone in diffractive processes.

The Wigner distribution depends on the transverse momentum $\vec{k}_\perp$ of partons as well as the impact parameter $\vec{b}_\perp$, including a dependence on the azimuthal angle between the two transverse vectors. In the GTMD approach this translates into a dependence on $\vec{k}_\perp$ and $\vec{\Delta}_\perp$. This dependence gives rise to a so-called elliptic Wigner function or GTMD [9]. In the region of small-x which is of interest in this paper, the equivalent color dipole approach for diffractive processes [10, 11] can be used. Here, the dipole amplitude depending on dipole size $\vec{r}_\perp$ and impact parameter $\vec{b}_\perp$ contains the same information as the Wigner function/GTMD. The azimuthal angle correlation discussed above translates then into a dependence on the dipole orientation with respect to the background color field of the target.

JHEP10(2023)179

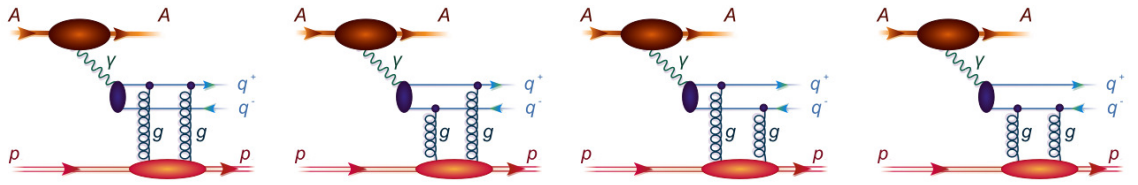

Figure 1. Feynman diagrams for the diffractive photoproduction of $q\bar{q}$ pairs in nucleus-proton collisions, discussed in the present paper.

In inclusive processes this dependence can give rise to flow-like azimuthal correlations, for example in prompt photons production [12], or in inclusive two-particles' production [13].

It was advocated that the elliptic gluon distributions could be studied in diffractive reactions, such as:

- Exclusive dijet production in ep collisions [14, 15]. For calculations in the color dipole approach, see [16–18];
- Exclusive dijet photoproduction in pA and AA ultra-peripheral collisions (UPCs) [19];
- Exclusive $Q\bar{Q}$ (with $Q = c, b$) photoproduction in pA and AA UPCs [20].

Here, we revisit the exclusive production of $c\bar{c}$ pairs in proton-lead collisions at LHC energies. The dominant reaction mechanism here is the diffractive photoproduction of the $c\bar{c}$ pair on a proton by a Weizsäcker-Williams photon emitted by the lead nucleus, see the diagrams in figure 1. One is then interested in the correlations of

$$\vec{P}_\perp = \frac{1}{2}(\vec{p}_{\perp Q} - \vec{p}_{\perp \bar{Q}})\,, \tag{1.1}$$

and the momentum transfer to the proton, which for the exclusive reaction fulfills

$$\vec{\Delta}_\perp = \vec{p}_{\perp Q} + \vec{p}_{\perp \bar{Q}}\,. \tag{1.2}$$

In this work we account only for the contribution where the ion serves as a source of the photon. Here we exploit the fact, that the photon flux scales with the charge of the ion as Z^2. This factor will be missing when the photon is emitted by the proton. On the other hand, the integrated diffractive process on the nucleus will display a dependence $\sigma \propto A^\alpha$, with roughly $\alpha \sim 1.4 \div 1.5$ (see e.g. [1, 3]). While the diffractive photoproduction on the nucleus may therefore still be a sizeable effect, the extraction of the process discussed in this paper is possible if proton tagging [21–23] is available, due to the very sharp transverse momentum dependence of the electromagnetically scattered proton.

In distinction to dijet production, for the heavy quarks already the quark mass m_Q can play the role of a hard scale, and also intermediate and small values of $\vec{P}_\perp$ are tractable. Here, we will calculate cross sections and distributions for realistic kinematic conditions at the LHC. We also discuss some subtleties regarding the correlations in the azimuthal angle

$$\cos\phi = \frac{\vec{P}_\perp \cdot \vec{\Delta}_\perp}{P_\perp \Delta_\perp}\,. \tag{1.3}$$

JHEP10(2023)179

At large jet momenta $P_\perp$ the correlations in ϕ expected to be dominantly $\propto \cos(2\phi)$ and are unambiguously expressed in terms of the elliptic Wigner function/GTMD. At lower $P_\perp$, however, the azimuthal correlations are better understood as coming from the matrix element (or impact factor) at finite $\Delta_\perp$. While formally also these correlations can be absorbed into the Wigner function/GTMD, these would correspond to δ-function terms in the latter. We discuss the relation between the different approaches and the alternative formulation in terms of a off-forward gluon density matrix introduced in ref. [24].

This paper is organized as follows. In section 2, we explain how to calculate the diffractive cross section of interest and discuss the formalism starting from the dipole representation of the amplitude. Then, in section 3 we present our numerical results for differential cross sections as functions of various kinematical variables using a variety of the existing gluon GTMD models. Finally, in section 4 the main conclusions are summarised.

2 Formalism

2.1 Kinematics and cross section

The cross section for the proton-nucleus reaction can be written in the following form

$$\frac{d\sigma(pA \to Q\bar{Q}pA; s)}{dx_Q dx_{\bar{Q}} d^2\vec{P}_\perp d^2\vec{\Delta}_\perp} = \frac{1}{x_Q + x_{\bar{Q}}} f_{\gamma/A}(x_Q + x_{\bar{Q}}) \frac{d\sigma(\gamma p \to Q\bar{Q}p; (x_Q + x_{\bar{Q}})s)}{dz d^2\vec{P}_\perp d^2\vec{\Delta}_\perp}, \tag{2.1}$$

with $z = x_Q/(x_Q + x_{\bar{Q}})$. Here, x_Q, $x_{\bar{Q}}$ are the fractions of the nucleus' Light-Front plus momentum carried by a heavy quark Q and antiquark $\bar{Q}$ (with mass m_Q), respectively. The transverse momenta of quark and antiquark are

$$\vec{p}_{\perp Q} = \vec{P}_\perp + \frac{\vec{\Delta}_\perp}{2}, \qquad \vec{p}_{\perp \bar{Q}} = -\vec{P}_\perp + \frac{\vec{\Delta}_\perp}{2}, \tag{2.2}$$

respectively, so that $\vec{\Delta}_\perp$ is the transverse momentum of the $Q\bar{Q}$ pair. As the photon is collinear to the incoming nucleus, $\vec{\Delta}_\perp$ is also equal, up to a sign, to the transverse momentum transfer to the proton target.

The Weizsäcker-Williams photons carry the momentum fraction

$$x_A = x_Q + x_{\bar{Q}}\,. \tag{2.3}$$

For the flux of quasireal photons,

$$f_{\gamma/A}(x_A) = \frac{dN(x_A)}{dx_A}, \tag{2.4}$$

we use the well-known expression (see for example the review [25]),

$$\frac{dN(x_A)}{dx_A} = \frac{2Z^2\alpha_{\rm em}}{\pi x_A}\left[\xi_{jA}K_0(\xi_{jA})K_1(\xi_{jA}) - \frac{\xi_{jA}^2}{2}(K_1^2(\xi_{jA}) - K_0^2(\xi_{jA}))\right], \tag{2.5}$$

where Z correspond to the atomic number of the projectile particle, $\alpha_{\rm em}$ is the fine structure constant, $\xi_{jA} = x_A m_p(R_j + R_A)$ involves the target and nucleus radii (R_j and R_A,

JHEP10(2023)179

respectively) and effectively excludes the overlap of the projectile and the target in impact parameter space, and m_p is the proton mass.

Let us also quote a useful expression for the cross section which reads in terms of center-of-mass rapidities y_Q, $y_{\bar{Q}}$ of quarks,

$$\frac{d\sigma(pA \to Q\bar{Q}pA; s)}{dy_Q dy_{\bar{Q}} d^2\vec{P}_\perp d^2\vec{\Delta}_\perp} = x_A \frac{dN(x_A)}{dx_A} \left(z(1-z) \frac{d\sigma(\gamma p \to Q\bar{Q}p; x_A s)}{dz d^2\vec{P}_\perp d^2\vec{\Delta}_\perp} \right) \Bigg|_{z=\frac{x_Q}{x_A}}, \tag{2.6}$$

where

$$x_Q = \sqrt{\frac{p_{\perp Q}^2 + m_Q^2}{s}} \exp(y_Q), \qquad x_{\bar{Q}} = \sqrt{\frac{p_{\perp \bar{Q}}^2 + m_Q^2}{s}} \exp(y_{\bar{Q}}). \tag{2.7}$$

We also need the transverse mass of the $Q\bar{Q}$-pair, which square is given by

$$M_\perp^2 = x_A \left(\frac{p_{\perp Q}^2 + m_Q^2}{x_Q} + \frac{p_{\perp \bar{Q}}^2 + m_Q^2}{x_{\bar{Q}}} \right). \tag{2.8}$$

The rapidity of the $Q\bar{Q}$-pair in the cm-frame can then be calculated from

$$Y_{\rm pair} = \frac{1}{2} \log\left(\frac{x_A}{x_B}\right) = \log\left(\frac{x_A\sqrt{s}}{M_\perp}\right), \qquad x_A x_B s = M_\perp^2. \tag{2.9}$$

We will be also interested in the laboratory frame rapidities, which are obtained from the shift

$$y_{Q,\bar{Q}}^{\rm LAB} = y_{Q,\bar{Q}} + \frac{1}{2}\log\left(\frac{Z}{A}\right), \quad Y_{\rm pair}^{\rm LAB} = Y_{\rm pair} + \frac{1}{2}\log\left(\frac{Z}{A}\right), \tag{2.10}$$

where for the ^{208}Pb nucleus, we have $A = 208$, $Z = 82$.

2.2 Color dipole representation of the diffractive amplitude

We start our discussion from a basic description of the color dipole approach to diffractive processes [10, 11]. Here, the cross section for the $\gamma p \to Q\bar{Q}$ diffractive dissociation process is written as

$$\frac{d\sigma(\gamma p \to Q\bar{Q}p; s_{\gamma p})}{dz d^2\vec{P}_\perp d^2\vec{\Delta}_\perp} = \overline{\sum_{\lambda_\gamma,\lambda,\bar{\lambda}} \left| \int \frac{d^2\vec{b}_\perp d^2\vec{r}_\perp}{(2\pi)^2} e^{-i\vec{\Delta}_\perp\cdot\vec{b}_\perp} e^{-i\vec{P}_\perp\cdot\vec{r}_\perp} N(Y, \vec{r}_\perp, \vec{b}_\perp)\, \Psi_{\lambda\bar{\lambda}}^{\lambda_\gamma}(z, \vec{r}_\perp) \right|^2}. \tag{2.11}$$

Above, z, $1-z$ are the Light-Front momentum fractions carried by quark/antiquark in the $\gamma \to Q\bar{Q}$ transition. The corresponding Light-Front wave function for the $\gamma \to Q\bar{Q}$,

$$\Psi_{\lambda\bar{\lambda}}^{\lambda_\gamma}(z, \vec{r}_\perp) = \frac{1}{\sqrt{4\pi z(1-z)}} \int \frac{d^2\vec{l}_\perp}{(2\pi)^2} e^{i\vec{r}_\perp\cdot\vec{l}_\perp}\, \Psi_{\lambda\bar{\lambda}}^{\lambda_\gamma}(z, \vec{l}_\perp), \tag{2.12}$$

depends on the Light-Front helicities of quarks, $\lambda/2$, $\bar{\lambda}/2$ and photon, λ_γ. Its explicit form in transverse momentum space can be found for example in ref. [26].

JHEP10(2023)179

Our main interest is in the dipole scattering amplitude $N(Y,\vec{r}_\perp,\vec{b}_\perp)$. Its energy dependence is encoded through the "rapidity" Y. We define the latter as $Y=\ln(x_0/x_{\mathbb{P}})$, with $x_0=0.01$. Here,

$$x_{\mathbb{P}}\equiv x_B=\frac{M_\perp^2}{s_{\gamma p}}=\frac{M_\perp^2}{x_A s}\,, \tag{2.13}$$

where $M_\perp$ is the transverse mass of the $Q\bar{Q}$ system. The dipole amplitude is related to the familiar color dipole cross section (see e.g. the textbook [27]) via

$$\sigma(x_{\mathbb{P}},\vec{r}_\perp)=2\int d^2\vec{b}_\perp\, N(Y,\vec{r}_\perp,\vec{b}_\perp)\,. \tag{2.14}$$

It is related to an off-diagonal generalization of the unintegrated gluon distribution — a gluon density matrix through the relation [24]:

$$\begin{aligned}N(Y,\vec{r}_\perp,\vec{b}_\perp)=&\int d^2\vec{q}_\perp d^2\vec{\kappa}_\perp\, f\left(Y,\frac{\vec{q}_\perp}{2}+\vec{\kappa}_\perp,\frac{\vec{q}_\perp}{2}-\vec{\kappa}_\perp\right)\exp[i\vec{q}_\perp\cdot\vec{b}_\perp]\\&\times\left\{\exp\left[i\frac{1}{2}\vec{q}_\perp\cdot\vec{r}_\perp\right]+\exp\left[-i\frac{1}{2}\vec{q}_\perp\cdot\vec{r}_\perp\right]-\exp[i\vec{\kappa}_\perp\cdot\vec{r}_\perp]-\exp[-i\vec{\kappa}_\perp\cdot\vec{r}_\perp]\right\}\,.\end{aligned} \tag{2.15}$$

Quark and antiquark move at impact parameters,

$$\vec{b}_{\perp Q}=\vec{b}_\perp+\frac{\vec{r}_\perp}{2}\,,\qquad \vec{b}_{\perp\bar{Q}}=\vec{b}_\perp-\frac{\vec{r}_\perp}{2}\,, \tag{2.16}$$

which allow us to relate the four phase factors in the curly bracket in eq. (2.15) to the four diagrams of figure 1 in an obvious fashion. We write the unintegrated gluon density matrix in the following form,

$$f\left(Y,\frac{\vec{q}_\perp}{2}+\vec{\kappa}_\perp,\frac{\vec{q}_\perp}{2}-\vec{\kappa}_\perp\right)=\frac{\alpha_s}{4\pi N_{\rm c}}\frac{\mathcal{F}\left(x_{\mathbb{P}},\frac{\vec{q}_\perp}{2}+\vec{\kappa}_\perp,\frac{\vec{q}_\perp}{2}-\vec{\kappa}_\perp\right)}{\left(\frac{\vec{q}_\perp}{2}+\vec{\kappa}_\perp\right)^2\left(\frac{\vec{q}_\perp}{2}-\vec{\kappa}_\perp\right)^2}\,, \tag{2.17}$$

where $N_{\rm c}=3$ for the number of colors in QCD, and we put in evidence the strong coupling constant α_s and gluon propagators here.

Integrating eq. (2.15) over $\vec{b}_\perp$, we obtain for the dipole cross section the well-known representation [28]

$$\sigma(x_{\mathbb{P}},\vec{r}_\perp)=\frac{2\pi}{N_{\rm c}}\int\frac{d^2\vec{\kappa}_\perp}{\kappa_\perp^4}\alpha_s\mathcal{F}(x_{\mathbb{P}},\vec{\kappa}_\perp,-\vec{\kappa}_\perp)\left\{2-e^{i\vec{\kappa}_\perp\cdot\vec{r}_\perp}-e^{-i\vec{\kappa}_\perp\cdot\vec{r}_\perp}\right\}\,, \tag{2.18}$$

so that indeed $\mathcal{F}(x,\vec{\kappa}_{\perp 1},\vec{\kappa}_{\perp 2})$ is the proper off-forward generalization of the standard unintegrated gluon distribution, which relates to its collinear counterpart via

$$xg(x,\mu^2)=\int\frac{d^2\vec{\kappa}_\perp}{\pi\kappa_\perp^2}\,\theta(\mu^2-\kappa_\perp^2)\,\mathcal{F}(x,\vec{\kappa}_\perp,-\vec{\kappa}_\perp)\,. \tag{2.19}$$

Below, we will also use the non-perturbative parameter,

$$\sigma_0(x_{\mathbb{P}})=\frac{4\pi}{N_{\rm c}}\int\frac{d^2\vec{\kappa}_\perp}{\kappa_\perp^4}\alpha_s\mathcal{F}(x_{\mathbb{P}},\vec{\kappa}_\perp,-\vec{\kappa}_\perp)\,, \tag{2.20}$$

which has the interpretation of the dipole cross section for large dipoles.

JHEP10(2023)179

Now, inserting the representation of the dipole amplitude given in eq. (2.15) into eq. (2.11), we obtain for the diffractive amplitude the following convolution structure:

$$\mathcal{A}(Y,\vec{P}_\perp,\vec{\Delta}_\perp) \propto \int d^2\vec{\kappa}_\perp\, f\left(Y,\frac{\vec{\Delta}_\perp}{2}+\vec{\kappa}_\perp,\frac{\vec{\Delta}_\perp}{2}-\vec{\kappa}_\perp\right)\left\{\Psi^{\lambda_\gamma}_{\lambda\bar{\lambda}}\left(z,\vec{P}_\perp+\frac{\vec{\Delta}_\perp}{2}\right)+\Psi^{\lambda_\gamma}_{\lambda\bar{\lambda}}\left(z,\vec{P}_\perp-\frac{\vec{\Delta}_\perp}{2}\right)\right.$$
$$\left.-\Psi^{\lambda_\gamma}_{\lambda\bar{\lambda}}(z,\vec{P}_\perp+\vec{\kappa}_\perp)-\Psi^{\lambda_\gamma}_{\lambda\bar{\lambda}}(z,\vec{P}_\perp-\vec{\kappa}_\perp)\right\}. \tag{2.21}$$

Here, in the terminology of small-x (or BFKL) factorization, one would refer to the structure in brackets as the impact factor for the coupling of two off-shell gluons to the $\gamma\to Q\bar{Q}$ amplitude. The two t-channel gluons carry the transverse momenta,

$$\vec{\kappa}_{\perp 1}=\frac{\vec{\Delta}_\perp}{2}+\vec{\kappa}_\perp,\quad \vec{\kappa}_{\perp 2}=\frac{\vec{\Delta}_\perp}{2}-\vec{\kappa}_\perp\,, \tag{2.22}$$

and the impact factor has the property that it vanishes when either of the gluon transverse momenta goes to zero, i.e. for $\vec{\kappa}_\perp=\pm\vec{\Delta}_\perp/2$.

Finally, we obtain for our diffractive photoproduction cross section:

$$\frac{d\sigma(\gamma p\to Q\bar{Q}p;s_{\gamma p})}{dz d^2\vec{P}_\perp d^2\vec{\Delta}_\perp}=e_f^2\alpha_{\rm em}\,2N_c(2\pi)^2\left\{\left(z^2+(1-z)^2\right)\left|\vec{\mathcal{M}}_0\right|^2+m_Q^2\left|\mathcal{M}_1\right|^2\right\}. \tag{2.23}$$

Here, $\mathcal{M}_1$ and $\vec{\mathcal{M}}_0$ are amplitudes for the sum of quark helicities equal to one or zero, respectively. Explicitly, we find (see e.g. ref. [29]):

$$\vec{\mathcal{M}}_0(\vec{P}_\perp,\vec{\Delta}_\perp)=\int\frac{d^2\vec{k}_\perp}{2\pi}\,f\left(Y,\frac{\vec{\Delta}_\perp}{2}+\vec{k}_\perp,\frac{\vec{\Delta}_\perp}{2}-\vec{k}_\perp\right)\left\{\frac{\vec{P}_\perp-\vec{\Delta}_\perp/2}{(\vec{P}_\perp-\vec{\Delta}_\perp/2)^2+m_Q^2}\right.$$
$$\left.+\frac{\vec{P}_\perp+\vec{\Delta}_\perp/2}{(\vec{P}_\perp+\vec{\Delta}_\perp/2)^2+m_Q^2}-\frac{\vec{P}_\perp-\vec{k}_\perp}{(\vec{P}_\perp-\vec{k}_\perp)^2+m_Q^2}-\frac{\vec{P}_\perp+\vec{k}_\perp}{(\vec{P}_\perp+\vec{k}_\perp)^2+m_Q^2}\right\},$$
$$\mathcal{M}_1(\vec{P}_\perp,\vec{\Delta}_\perp)=\int\frac{d^2\vec{k}_\perp}{2\pi}\,f\left(Y,\frac{\vec{\Delta}_\perp}{2}+\vec{k}_\perp,\frac{\vec{\Delta}_\perp}{2}-\vec{k}_\perp\right)\left\{\frac{1}{(\vec{P}_\perp-\vec{\Delta}_\perp/2)^2+m_Q^2}\right.$$
$$\left.+\frac{1}{(\vec{P}_\perp+\vec{\Delta}_\perp/2)^2+m_Q^2}-\frac{1}{(\vec{P}_\perp-\vec{k}_\perp)^2+m_Q^2}-\frac{1}{(\vec{P}_\perp+\vec{k}_\perp)^2+m_Q^2}\right\}. \tag{2.24}$$

In order to understand the origin of azimuthal correlations, it is useful to decompose our amplitude. To this end, let us introduce

$$\vec{\mathcal{J}}_0(\vec{P}_\perp,\vec{q}_\perp)=\frac{\vec{P}_\perp-\vec{q}_\perp}{(\vec{P}_\perp-\vec{q}_\perp)^2+m_Q^2}+\frac{\vec{P}_\perp+\vec{q}_\perp}{(\vec{P}_\perp+\vec{q}_\perp)^2+m_Q^2}-\frac{2\vec{P}_\perp}{\vec{P}_\perp^2+m_Q^2},$$
$$\mathcal{J}_1(\vec{P}_\perp,\vec{q}_\perp)=\frac{1}{(\vec{P}_\perp-\vec{q}_\perp)^2+m_Q^2}+\frac{1}{(\vec{P}_\perp+\vec{q}_\perp)^2+m_Q^2}-\frac{2}{\vec{P}_\perp^2+m_Q^2}. \tag{2.25}$$

JHEP10(2023)179

Then, our matrix elements take the form:

$$\vec{\mathcal{M}}_0(\vec{P}_\perp,\vec{\Delta}_\perp)=\vec{\mathcal{J}}_0\left(\vec{P}_\perp,\frac{1}{2}\vec{\Delta}_\perp\right)C(Y,\vec{\Delta}_\perp)-\int\frac{d^2\vec{k}_\perp}{2\pi}\vec{\mathcal{J}}_0(\vec{P}_\perp,\vec{k}_\perp)\,f\left(Y,\frac{\vec{\Delta}_\perp}{2}+\vec{k}_\perp,\frac{\vec{\Delta}_\perp}{2}-\vec{k}_\perp\right),$$
$$\mathcal{M}_1(\vec{P}_\perp,\vec{\Delta}_\perp)=\mathcal{J}_1\left(\vec{P}_\perp,\frac{1}{2}\vec{\Delta}_\perp\right)C(Y,\vec{\Delta}_\perp)-\int\frac{d^2\vec{k}_\perp}{2\pi}\mathcal{J}_1(\vec{P}_\perp,\vec{k}_\perp)\,f\left(Y,\frac{\vec{\Delta}_\perp}{2}+\vec{k}_\perp,\frac{\vec{\Delta}_\perp}{2}-\vec{k}_\perp\right). \tag{2.26}$$

There emerges a rapidity-dependent form factor,

$$C(Y,\vec{\Delta}_\perp)=\int\frac{d^2\vec{k}_\perp}{2\pi}\,f\left(Y,\frac{\vec{\Delta}_\perp}{2}+\vec{k}_\perp,\frac{\vec{\Delta}_\perp}{2}-\vec{k}_\perp\right), \tag{2.27}$$

which is a non-perturbative parameter, as is obvious from its form in the forward limit as an integral,

$$C(Y,0)=\frac{1}{4\pi N_{\rm c}}\int\frac{d^2\vec{k}_\perp}{2\pi k_\perp^4}\,\alpha_s\mathcal{F}(x_{\mathbb{P}},\vec{k}_\perp,-\vec{k}_\perp), \tag{2.28}$$

that converges at soft, non-perturbative values of $k_\perp$. Indeed, as can be seen from eq. (2.20), it is directly proportional to the dipole cross section for large dipoles, $\sigma_0(x_{\mathbb{P}})$.

2.3 GTMD representation

In the literature, often a different momentum-space representation of the diffractive amplitude is used (see, for example, refs. [9, 19, 20]). Namely, one introduces the Fourier transform of the dipole amplitude (using the normalization and notation of ref. [20]),

$$T(Y,\vec{k}_\perp,\vec{\Delta}_\perp)=\int\frac{d^2\vec{b}_\perp}{(2\pi)^2}\frac{d^2\vec{r}_\perp}{(2\pi)^2}\,e^{-i\vec{\Delta}_\perp\cdot\vec{b}_\perp}\,e^{-i\vec{k}_\perp\cdot\vec{r}_\perp}\,N(Y,\vec{r}_\perp,\vec{b}_\perp). \tag{2.29}$$

Here, $T(Y,\vec{k}_\perp,\vec{\Delta}_\perp)$ is often referred to as the generalized transverse momentum distribution (GTMD) of gluons in the proton target. Certainly, just like the gluon density matrix $f\left(Y,\frac{\vec{q}_\perp}{2}+\vec{\kappa}_\perp,\frac{\vec{q}_\perp}{2}-\vec{\kappa}_\perp\right)$, it encodes the same information as the dipole amplitude. What is the relation between these two momentum space distributions?

To answer this question, let us perform the Fourier transform by inserting eq. (2.15) into eq. (2.29), which yields

$$\begin{aligned}T(Y,\vec{k}_\perp,\vec{\Delta}_\perp)=C(Y,\vec{\Delta}_\perp)&\left(\delta^{(2)}\left(\vec{k}_\perp-\frac{\vec{\Delta}_\perp}{2}\right)+\delta^{(2)}\left(\vec{k}_\perp+\frac{\vec{\Delta}_\perp}{2}\right)\right)\\&-f\left(Y,\frac{\vec{\Delta}_\perp}{2}+\vec{k}_\perp,\frac{\vec{\Delta}_\perp}{2}-\vec{k}_\perp\right)-f\left(Y,\frac{\vec{\Delta}_\perp}{2}-\vec{k}_\perp,\frac{\vec{\Delta}_\perp}{2}+\vec{k}_\perp\right),\end{aligned} \tag{2.30}$$

where $C(Y,\vec{\Delta}_\perp)$ of eq. (2.27) multiplies a combination of δ-functions. Now, evidently T is essentially equal to the f, up to the term containing δ-functions. The latter, however, will not contribute when convoluted with the impact factor in eq. (2.21). Formally, we might therefore replace

$$f\left(Y,\frac{\vec{\Delta}_\perp}{2}+\vec{k}_\perp,\frac{\vec{\Delta}_\perp}{2}-\vec{k}_\perp\right)\to-\frac{1}{2}\,T(Y,\vec{k}_\perp,\vec{\Delta}_\perp). \tag{2.31}$$

JHEP10(2023)179

In practical numerical applications, however, this equivalence is not that obvious. In diffractive interactions the values of $\Delta_\perp$ are bounded by the diffractive slope B_D, so that at large values of $k_\perp$ the delta-functions are irrelevant, and the two gluon distributions, f and T are equal to each other, up to a factor of $1/2$.

An immediate corollary of the representation in eq. (2.30) is the sum rule

$$\int d^2\vec{k}_\perp \, T(Y, \vec{k}_\perp, \vec{\Delta}_\perp) = 0 \,, \tag{2.32}$$

which encodes the fact, that $N(Y, \vec{r}_\perp, \vec{b}_\perp) \to 0$ for $r_\perp \to 0$. Generally speaking, as evidenced by the presence of δ-function terms, the Fourier transform is a non-convergent integral and does not exist as a function. One therefore needs to regularize the Fourier transform which is often done by inserting a Gaussian cutoff function [9, 19, 20]:

$$T(Y, \vec{k}_\perp, \vec{\Delta}_\perp) = \int \frac{d^2\vec{b}_\perp}{(2\pi)^2} \frac{d^2\vec{r}_\perp}{(2\pi)^2} e^{-i\vec{\Delta}_\perp \cdot \vec{b}_\perp} e^{-i\vec{k}_\perp \cdot \vec{r}_\perp} \, N(Y, \vec{r}_\perp, \vec{b}_\perp) \, e^{-\varepsilon r_\perp^2} \,. \tag{2.33}$$

Now, inserting the representation in eq. (2.15), we obtain the cutoff-dependent T as

$$\begin{aligned} T(Y, \vec{k}_\perp, \vec{\Delta}_\perp) = C(Y, \vec{\Delta}_\perp) \left(\delta_\varepsilon^{(2)} \left(\vec{k}_\perp - \frac{\vec{\Delta}_\perp}{2} \right) + \delta_\varepsilon^{(2)} \left(\vec{k}_\perp + \frac{\vec{\Delta}_\perp}{2} \right) \right) \\ - f_\varepsilon \left(Y, \frac{\vec{\Delta}_\perp}{2} + \vec{k}_\perp, \frac{\vec{\Delta}_\perp}{2} - \vec{k}_\perp \right) - f_\varepsilon \left(Y, \frac{\vec{\Delta}_\perp}{2} - \vec{k}_\perp, \frac{\vec{\Delta}_\perp}{2} + \vec{k}_\perp \right) \,, \end{aligned} \tag{2.34}$$

where

$$\delta_\varepsilon^{(2)}(\vec{k}_\perp) = \frac{1}{4\pi\varepsilon} \exp\left(-\frac{k_\perp^2}{4\varepsilon} \right) \,, \tag{2.35}$$

is a "smeared out" delta-distribution, and

$$f_\varepsilon \left(Y, \frac{\vec{\Delta}_\perp}{2} - \vec{k}_\perp, \frac{\vec{\Delta}_\perp}{2} + \vec{k}_\perp \right) = \int d^2\vec{\kappa}_\perp \, f \left(Y, \frac{\vec{\Delta}_\perp}{2} - \vec{\kappa}_\perp, \frac{\vec{\Delta}_\perp}{2} + \vec{\kappa}_\perp \right) \delta_\varepsilon^{(2)}(\vec{k}_\perp - \vec{\kappa}_\perp) \tag{2.36}$$

is a smeared out version of the gluon density matrix. The regularized T-matrix also fulfills the sum rule of eq. (2.32).

Let us finally quote the expressions of matrix elements $\vec{\mathcal{M}}_0$, $\mathcal{M}_1$ in terms of T, which read:

$$\begin{aligned} \vec{\mathcal{M}}_0 &= \int \frac{d^2\vec{k}_\perp}{2\pi} \, T(Y, \vec{k}_\perp, \vec{\Delta}_\perp) \left\{ \frac{\vec{P}_\perp - \vec{k}_\perp}{(\vec{P}_\perp - \vec{k}_\perp)^2 + m_Q^2} - \frac{\vec{P}_\perp}{\vec{P}_\perp^2 + m_Q^2} \right\} \,, \\ \mathcal{M}_1 &= \int \frac{d^2\vec{k}_\perp}{2\pi} \, T(Y, \vec{k}_\perp, \vec{\Delta}_\perp) \left\{ \frac{1}{(\vec{P}_\perp - \vec{k}_\perp)^2 + m_Q^2} - \frac{1}{\vec{P}_\perp^2 + m_Q^2} \right\} \,. \end{aligned} \tag{2.37}$$

In its derivation we made use of the sum rule of eq. (2.32). Notice, that in effect here we use the impact factor for forward scattering, and all dependence on $\vec{\Delta}_\perp$ has been absorbed into the GTMD $T(Y, \vec{k}_\perp, \vec{\Delta}_\perp)$.

JHEP10(2023)179

2.4 Benchmark gluon GTMDs

Let us briefly discuss the different GTMD models used in this work. We follow both approaches presented above, and consider a total of five different models as benchmarks in our analysis of the differential cross section of charm photoproduction in pA UPCs.

First, we use two different parametrizations of the off-forward gluon density matrix f of eq. (2.17). Here, we choose to write

$$f\left(Y, \frac{\vec{\Delta}_\perp}{2} + \vec{k}_\perp, \frac{\vec{\Delta}_\perp}{2} - \vec{k}_\perp\right) = \frac{\alpha_s}{4\pi N_c} \frac{\mathcal{F}(x_{\mathbb{P}}, \vec{k}_\perp, -\vec{k}_\perp)}{k_\perp^4} \exp\left[-\frac{1}{2} B \vec{\Delta}^2\right] . \tag{2.38}$$

Such a form has been suggested in ref. [30] for the case of vector meson production (for a recent use, see ref. [31]). The same approach has also been taken in ref. [12]. For the diffractive slope, we use $B = 4\,\mathrm{GeV}^{-2}$, and the diagonal unintegrated gluon distribution $\mathcal{F}$ is taken from two different models: the Golec-Biernat-Wüsthoff (GBW) model [32], and the Moriggi-Peccini-Machado (MPM) parametrization [33].

We also consider models based on the regularized Fourier transform of dipole amplitudes as in eq. (2.33). The first model is based on a numerical solution of the Balitsky-Kovchegov equation for the dipole S-matrix with impact parameter dependence [34, 35]. Such solutions have been obtained, for example in refs. [36–38]. In our work we use the results of ref. [9]. This solution is based on exploiting a symmetry first observed in [39]. We label it as HHU below.

The second model, based on the original effective McLerran-Venugopalan model of ref. [40], that has been generalised for the proton target and extended to incorporate inhomogeneities in the transverse-plane distribution of gluons in ref. [13]. The latter model has been applied for exclusive diffractive light and heavy quarks' photoproduction in refs. [19] and [20], respectively. We denote this model as MV-IR in what follows. A third model is the so-called bSat model of Kowalski and Teaney [41]. The Kowalski-Teaney (KT) model has been adjusted to the proton structure function data and hence it gives a rather realistic dipole amplitude. We use parameters from table I fit 3 of [41] for the gluon distribution. In this regard, the HHU and MV-IR models can be considered as rather toy models, they do, however, incorporate non-trivial dipole orientation effects, which is not the case for the KT model.

The leading dependence on dipole orientation is quantified by the elliptic part N_ϵ of the dipole amplitude in the Fourier expansion,

$$N(Y, \vec{r}_\perp, \vec{b}_\perp) = N_0(Y, r_\perp, b_\perp) + 2\,\cos(2\phi_{br})\, N_\epsilon(Y, r_\perp, b_\perp) + \dots . \tag{2.39}$$

We translate the isotropic and elliptic parts of the dipole amplitude to GTMDs by the appropriate Fourier-Bessel transforms [14, 19, 20]:

$$\begin{aligned} T_0(Y, k_\perp, \Delta_\perp) &= \frac{1}{4\pi^2} \int_0^\infty b_\perp db_\perp J_0(\Delta_\perp b_\perp) \int_0^\infty r_\perp dr_\perp J_0(k_\perp r_\perp)\, N_0(Y, r_\perp, b_\perp) e^{-\varepsilon r_\perp^2}, \\ T_\epsilon(Y, k_\perp, \Delta_\perp) &= \frac{1}{4\pi^2} \int_0^\infty b_\perp db_\perp J_2(\Delta_\perp b_\perp) \int_0^\infty r_\perp dr_\perp J_2(k_\perp r_\perp)\, N_\epsilon(Y, r_\perp, b_\perp) e^{-\varepsilon r_\perp^2} . \end{aligned} \tag{2.40}$$

JHEP10(2023)179

The explicit form of the matrix element for the elliptic glue for arbitrary quark mass m_Q has been found in ref. [20]. We briefly review its derivation in appendix A.

It is interesting to note that the gluon density matrices, constructed according to the prescription of eq. (2.38), do also lead to a dipole amplitude that depends on dipole orientation, as can be seen by plugging the expression of eq. (2.38) into eq. (2.15). It gives us the expression

$$N(Y,\vec{r}_\perp,\vec{b}_\perp)=\frac{1}{4}\left\{t_N\left(\vec{b}_\perp+\frac{\vec{r}_\perp}{2}\right)+t_N\left(\vec{b}_\perp-\frac{\vec{r}_\perp}{2}\right)-2t_N(\vec{b}_\perp)\right\}\sigma_0(x_{\mathbb{P}})+\frac{1}{2}t_N(\vec{b}_\perp)\sigma(x_{\mathbb{P}},\vec{r}_\perp)\,, \tag{2.41}$$

where

$$t_N(\vec{b}_\perp)=\int\frac{d^2\vec{q}_\perp}{(2\pi)^2}\,\exp(-i\vec{q}_\perp\cdot\vec{b}_\perp)\exp\left[-\frac{1}{2}Bq_\perp^2\right]\,. \tag{2.42}$$

Again, we see that the dipole orientation dependence appears together with the non-perturbative parameter σ_0 — the dipole cross section for large dipoles.

We want to stress, that the correlation between $\vec{r}_\perp$ and $\vec{b}_\perp$ emerges, although eq. (2.38) does not contain any correlation between $\vec{k}_\perp$ and $\vec{\Delta}_\perp$! The $\vec{r}_\perp\cdot\vec{b}_\perp$ correlation is in fact of a simple geometric origin, as it singles out the contributions of diagrams where only the quark or antiquark interact and probe the matter density at their respective impact parameters. There is no obvious way how to construct an off-forward glue that leads to totally isotropic dipole amplitude. For this to happen, the relevant dipole sizes simply have to be small enough for the matter density to be constant over distances $\sim r_\perp$. Then the shifts in the curly brackets do not matter and only the last term in eq. (2.41) effectively contributes. Of course, in general one would expect eq. (2.17) to have nontrivial azimuthal correlations between $\vec{k}_\perp$ and $\vec{\Delta}_\perp$, in which case the dipole amplitude will have a genuinely dynamical elliptic piece that can contribute also at hard momenta $\vec{P}_\perp$.

Finally, to wrap up this section, in figure 2 we show the $(\vec{k}_\perp,\vec{\Delta}_\perp)$ maps for various dipole-nucleon amplitudes $T(Y,\vec{k}_\perp,\vec{\Delta}_\perp)$ for comparison. In figure 3 we show for $x_{\mathbb{P}}=0.01$ and $\Delta_\perp=0.01\,\text{GeV}$ the function of eq. (2.38) for the GBW and MPM models, and the result of the Fourier transform eq. (2.40). Notice that the latter do change sign, in accordance with the sum rule eq. (2.32).

3 Numerical results

We now turn to our numerical results for the production of $c\bar{c}$ pairs. In this work, we use the charm quark mass value of $m_c=1.5\,\text{GeV}$. In this section, we show the cross-section distributions for $c\bar{c}$ photoproduction in pA UPCs differential in y_c^{LAB}, $Y_{\text{pair}}^{\text{LAB}}$, $x_{\mathbb{P}}$, as well as $P_\perp$, $\Delta_\perp$, t and ϕ, for several benchmark models of the gluon GTMD in the proton discussed above. We will show numerical results for differential distributions integrated over $0.01<P_\perp<10\,\text{GeV}$, as well as over $5<P_\perp<10\,\text{GeV}$ domains of the phase space. For all distributions calculated as Fourier transforms of $N(Y,\vec{r}_\perp,\vec{b}_\perp)$ (see eq. (2.33)) we use the same regularization parameter $\varepsilon=(0.5\,\text{fm})^{-2}$ as in ref. [20]. In table 1, we show our results for the integrated cross section for $P_\perp<10\,\text{GeV}$ as well as for $5<P_\perp<10\,\text{GeV}$. In addition we show results for $x_{\mathbb{P}}<0.05$. The results with the extra cut are only slightly

JHEP10(2023)179

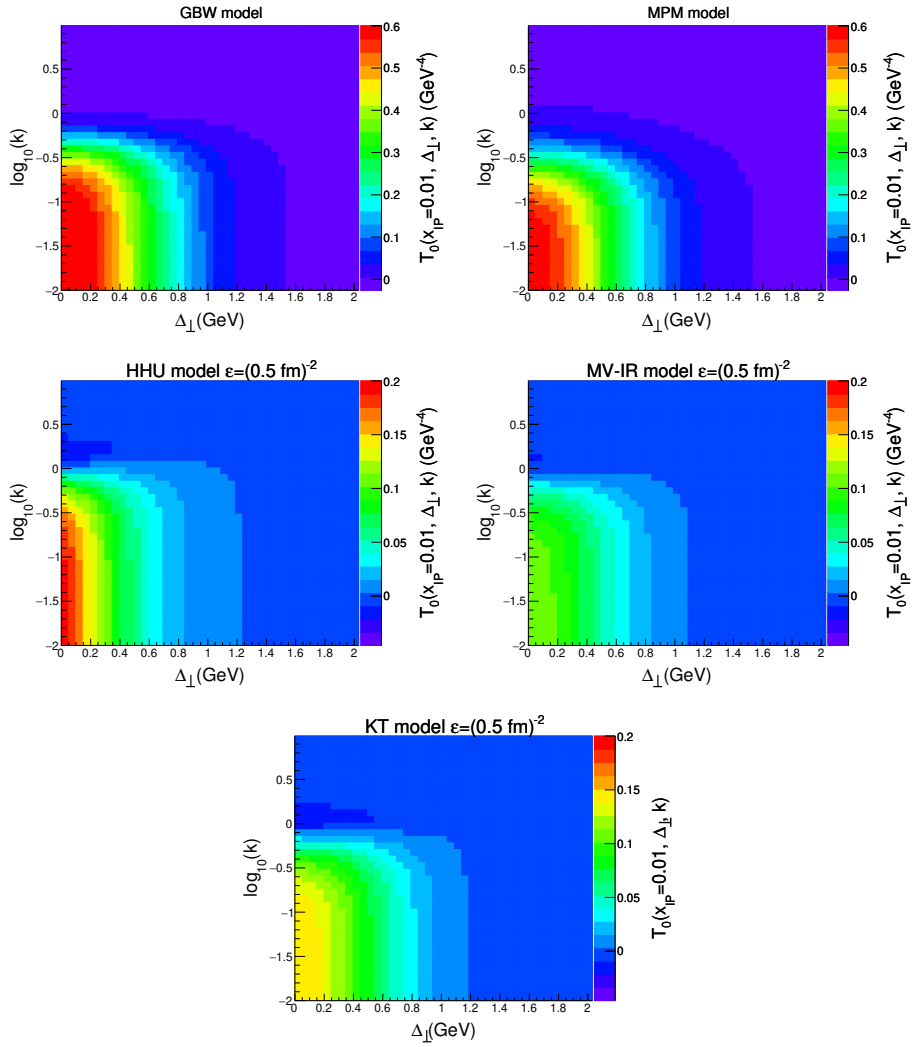

Figure 2. Different parametrizations for the gluon distribution in the proton.

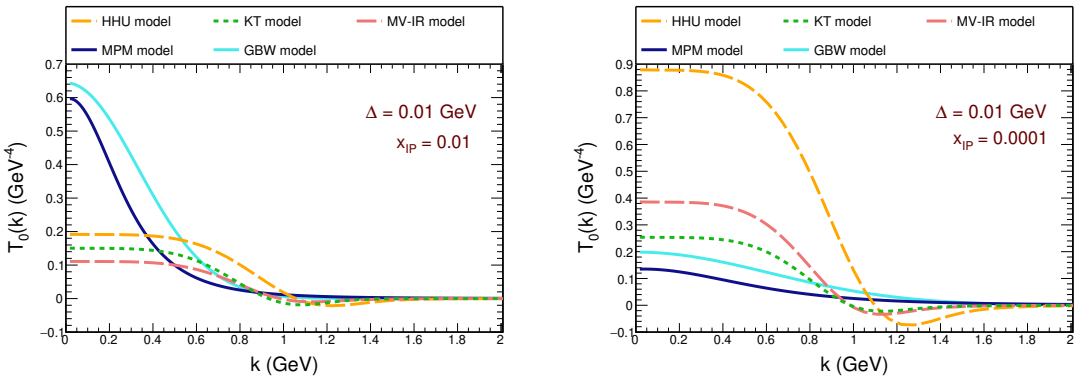

Figure 3. Different parametrizations for the gluon distribution in the proton for $\Delta = 0.01\,\text{GeV}$ and $x_{\mathbb{P}} = 0.01$ (on the left side) as well as $x_{\mathbb{P}} = 0.0001$ (on the right side). For the HHU, KT and MV-IR models, the regularization parameter $\varepsilon = (0.5\,\text{fm})^{-2}$ was chosen.

JHEP10(2023)179

	$x_{\mathbb{P}} < 1.0$		$x_{\mathbb{P}} < 0.05$	
GTMD approaches	σ [μb]	$\sigma_{P_\perp > 5.0\,\mathrm{GeV}}$ [μb]	σ [μb]	$\sigma_{P_\perp > 5.0\,\mathrm{GeV}}$ [μb]
GBW	335.199	0.051	330.046	0.046
MPM	321.141	0.201	293.300	0.173
$\varepsilon = (0.5\,\mathrm{fm})^{-2}$				
HHU	520.691	4.573	520.691	4.573
KT	66.699	0.111	65.023	0.110
MV-IR	136.675	0.606	129.883	0.526
$\varepsilon = \frac{1}{2}(0.5\,\mathrm{fm})^{-2}$				
HHU	743.411	4.348	743.411	4.348
KT	85.487	0.106	83.039	0.105
MV-IR	169.561	0.587	161.360	0.510

Table 1. Total cross section for $0.01 < P_\perp < 10.0\,\mathrm{GeV}$ and for $5.0 < P_\perp < 10.0\,\mathrm{GeV}$ and different approaches. In this table, the cross sections are integrated over $\Delta_\perp < 3\,\mathrm{GeV}$ and $-8 < y_c < 8$.

smaller, except of the MPM model. In table 1 we also varied the parameter ε by a factor two in order to give an estimate on the dependence on ε, which turns out to be rather large.

We notice considerable differences for the different GTMDs at large transverse momenta. For instance, the GBW distribution drops off with transverse momentum uch faster than other GTMDs. This is due to the fact that the GBW UGD does not possess the perturbative power-law tail at large momenta, but rather features a Gaussian distribution in transverse momenta with an x-dependent width. It should also be noted that the original MV-IR distribution is formulated in ref. [13] without $x_{\mathbb{P}}$ (or Y) dependence. To get semi-realistic results for the differential distributions, the original MV-IR has been modified as

$$T^{\mathrm{mod}}_{\text{MV-IR}}(Y, \vec{k}_\perp, \vec{\Delta}_\perp) = T_{\text{MV-IR}}(\vec{k}_\perp, \vec{\Delta}_\perp)\, e^{\lambda Y}, \quad Y = \ln\left(\frac{0.01}{x_{\mathbb{P}}}\right), \tag{3.1}$$

with $\lambda = 0.277$. It should be noted that more realistic extensions of the MV-IR model have been proposed in the literature, see e.g. [42].

We start our presentation from the lab-frame rapidity distributions of charm quarks in figure 4. Here, the incoming nucleus has a large positive rapidity, and the proton — a large negative rapidity. The range of the rapidity distribution at large y_c^{LAB} is essentially controlled by the photon flux. We see that the HHU GTMD leads to a significantly higher peak in the charm rapidity distribution than other models, and extends at the negative side only to $y_c^{\mathrm{LAB}} \sim -4$. This is due to the fact that it has a support only for small $x_{\mathbb{P}} < 0.01$. The GBW distribution gives results consistent with an earlier calculation of Gonçalves et al. [43], where only rapidity distributions were studied. In addition, the distributions in lab-frame rapidity of the $c\bar{c}$-pair are shown in figure 5. They rather closely resemble the single-quark rapidity distributions. The related $x_{\mathbb{P}}$ distributions are presented in figure 6.

JHEP10(2023)179

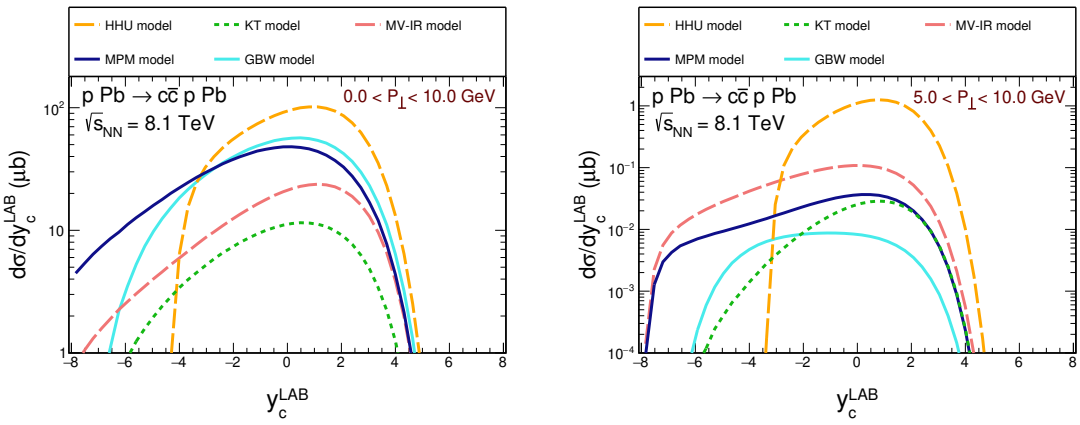

Figure 4. Distributions in lab-frame rapidity of the charm quark y_c^{LAB} for $0.01 < P_\perp < 10.0\,\mathrm{GeV}$ on the left and for $5.0 < P_\perp < 10.0\,\mathrm{GeV}$ on the right.

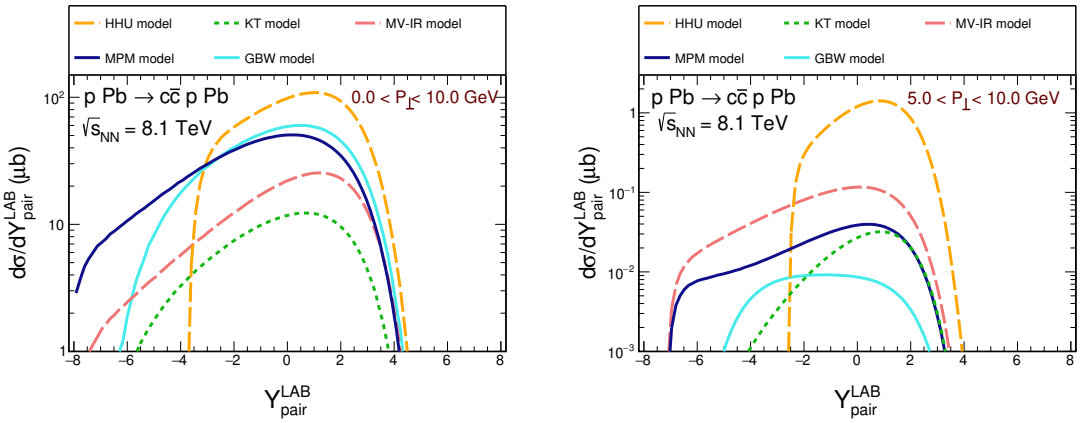

Figure 5. Distributions in rapidity of the $c\bar{c}$ pair Y_{pair} for $0.01 < P_\perp < 10.0\,\mathrm{GeV}$ on the left and for $5.0 < P_\perp < 10.0\,\mathrm{GeV}$ on the right.

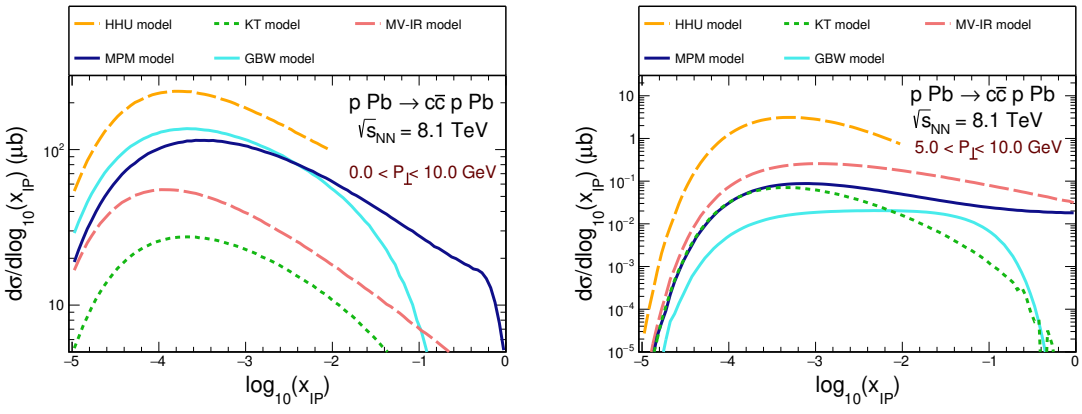

Figure 6. Distributions in $\log_{10}(x_{\mathbb{P}})$ for $0.01 < P_\perp < 10.0\,\mathrm{GeV}$ on the left and for $5.0 < P_\perp < 10.0\,\mathrm{GeV}$ on the right.

JHEP10(2023)179

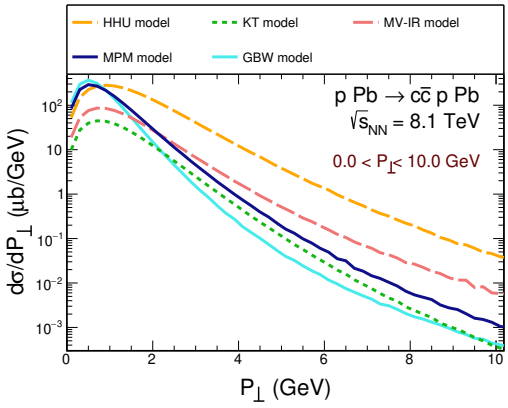

Figure 7. Distributions in $P_\perp$.

Values of $x_{\mathbb{P}}$ as small as 10^{-5} enter the calculation. Note that in the case of HHU GTMD, we assumed that this distribution only applies for $x_{\mathbb{P}} < 0.01$.

A comment on the range of the $x_{\mathbb{P}}$ distributions is in order. Notice, that the diffractively scattered proton will carry a fraction $\xi \approx 1 - x_{\mathbb{P}}$ of the beam momentum. Also, the rapidity gap between the products of photon dissociation rises at small $x_{\mathbb{P}}$ as $\propto \log(1/(1-\xi)) \sim \log(1/x_{\mathbb{P}})$. It is therefore clear that an experiment, which tags protons carrying a sizeable fraction of the beam momentum, would provide an upper limit on $x_{\mathbb{P}}$. For a discussion of relevant forward detectors at the LHC, see [21–23]. This goes together with considerations on the applicability of the dipole amplitudes used in this paper. This will in general require a large rapidity gap as mentioned above. There will be no sharp value of $x_{\mathbb{P}}$ where the dipole approach breaks down, but one would expect it to require $x_{\mathbb{P}} \ll 0.1$, with a conservative upper limit of $x_{\mathbb{P}} < 0.05$. In absence of concrete experimental conditions, below we will integrate over the whole phase space, i.e. up to $x_{\mathbb{P}}^{\max} = 1$, expecting that the impact from large $x_{\mathbb{P}}$ to the integrals is in general small. An exception are the distributions in rapidity, where large negative rapidities are close to the proton beam, and therefore associated with small gaps. We return to this issue at the end of this section, where we demonstrate the role of a cutoff $x_{\mathbb{P}}^{\max}$ on the various distributions.

We observe that the cut due to ε in eq. (2.40) has a different impact for different models. In particular, it has a strong effect on the KT model in the region of small P_T, where the bulk of the cross section resides. This makes the distributions integrated over P_T for the KT model very small. For $P_T > 2\,\text{GeV}$, however the results are comparable to other models. Eventually the value of the ε could be adjusted to experimental data.

Let us now term to transverse momentum distributions of the produced charm quarks. In figure 7 we show the differential distributions in $P_\perp$. We notice a considerable difference in the tail of the distributions, with the GBW glue giving the softest behaviour as expected. In figure 8 we present the charm distribution in $\Delta_\perp$. As generically anticipated for diffractive scattering, such a distribution is peaked at low values of $\Delta_\perp \sim 1/\sqrt{B}$, with B being the diffractive slope. The HHU model somewhat stands out as it gives rise to a peak in $\Delta_\perp$ distribution that is shifted to a softer value than that for the other GTMD models consid-

JHEP10(2023)179

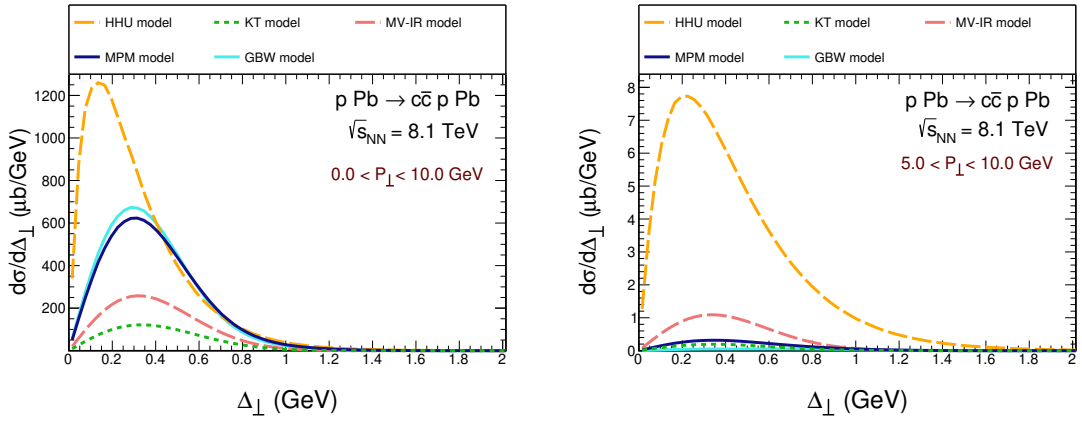

Figure 8. Distributions in $\Delta_\perp$ for $0.01 < P_\perp < 10.0\,\text{GeV}$ on the left and for $5.0 < P_\perp < 10.0\,\text{GeV}$ on the right.

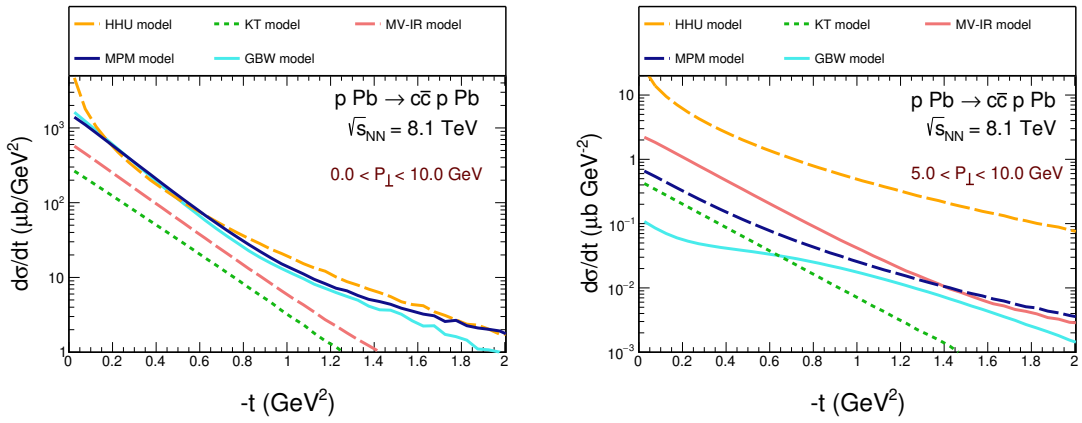

Figure 9. Distributions in $-t$ for $0.01 < P_\perp < 10.0\,\text{GeV}$ on the left and for $5.0 < P_\perp < 10.0\,\text{GeV}$ on the right.

ered in this work. These distributions are the result of the dynamics of gluons encoded in the BK equation. Presumably the behaviour of the $\Delta_\perp$ distribution could be made more realistic by introducing a similar regulator function in the impact parameter variable $b_\perp$ as in eq. (2.40) for the dipole size $r_\perp$. Here however we restrain from introducing additional parameters.

Next, in figure 9, we show the distribution in the Mandelstam variable

$$t = -\frac{\Delta_\perp^2 + x_{\mathbb{P}}^2 m_p^2}{1 - x_{\mathbb{P}}} \tag{3.2}$$

at the proton side. We see the typical diffractive peak for the $P_\perp$-integrated case. Again, the HHU model stands out with a noticeable curvature and very sharp forward peaking. In the large-$P_\perp$ tail, the t-distribution flattens out considerably for all considered GTMD benchmark models. Notice that this case corresponds to a rather large diffractive mass and, therefore, to a sizeable longitudinal momentum transfer.

JHEP10(2023)179

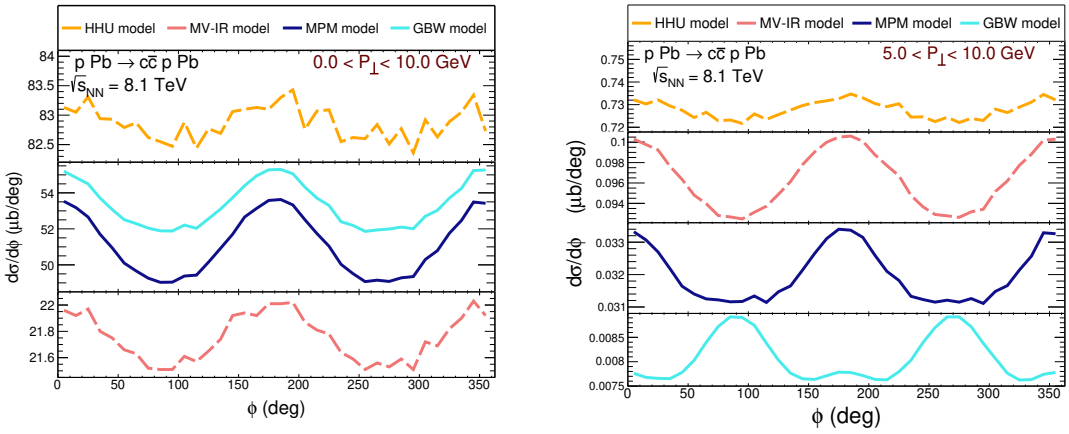

Figure 10. Distributions in the azimuthal angle ϕ between $\vec{P}_\perp$ and $\vec{\Delta}_\perp$ for $0.01 < P_\perp < 10.0\,\text{GeV}$ on the left and for $5.0 < P_\perp < 10.0\,\text{GeV}$ on the right.

We now turn to the angular correlations in azimuthal angle ϕ between $\vec{P}_\perp$ and $\vec{\Delta}_\perp$, shown in figure 10, which are one of the main results of this work. There are in general clearly visible correlations. Notice that for the GBW and MPM GTMDs these correlations are of the "geometric" origin, such that in momentum space they are fully generated by the matrix element. The angular modulations obtained from the GBW or MPM GTMDs are of order 10%. We observe that at large $P_\perp$ they quickly drop and change shape. Notice, that the calculations with these two GTMDs include all possible harmonics, not only $\cos 2\phi$. In the case when these correlations are computed accounting for the elliptic gluon distribution only (see eq. (2.33)), i.e. when only $\cos 2\phi$ modulations are included, they appear to be at the level of about 1–5%.

In order to better visualize the strength of the azimuthal correlations in figure 11, we present also the angular distributions divided by the integrated cross section for a given GTMD model. Such normalised distributions are easier to compare for different GTMDs. Again, we show the results for two ranges of $P_\perp$ as explained in the figure. The azimuthal modulations are of the order of a few percent.

Let us return to the issue on a cutoff in $x_{\mathbb{P}}$. In figures 12, 13, 14 we show the effect of introducing an upper limit $x_{\mathbb{P}}^{\max}$ into our integration by example of three distributions. Here we used the MPM model for the GTMD. In figure 12 we clearly see the expected effect of the cutoff on the distribution at large negative rapidities, beyond $y_c^{\text{LAB}} \sim -4$ the cross section quickly drops. The effect of the cutoff is more marked in the high $P_\perp$ domain as seen from the right panel. The $\Delta_\perp$ distribution shown in figure 13 is rather mildly affected, with again a stronger effect at large $P_\perp$. Finally, the distribution in the azimuthal angle ϕ shown in figure 14 is practically unaffected.

As these are parton-level observables, these angular distributions are not directly measurable. For the case of dijets, one would expect soft-gluon corrections to have an impact, see e.g. ref. [44]. For the more relevant case of exclusive (or inclusive diffractive) pairs of open heavy flavor mesons (D-mesons), a thorough study of hadronization corrections would be required. Such a study however goes beyond the scope of the present work. Recently,

JHEP10(2023)179

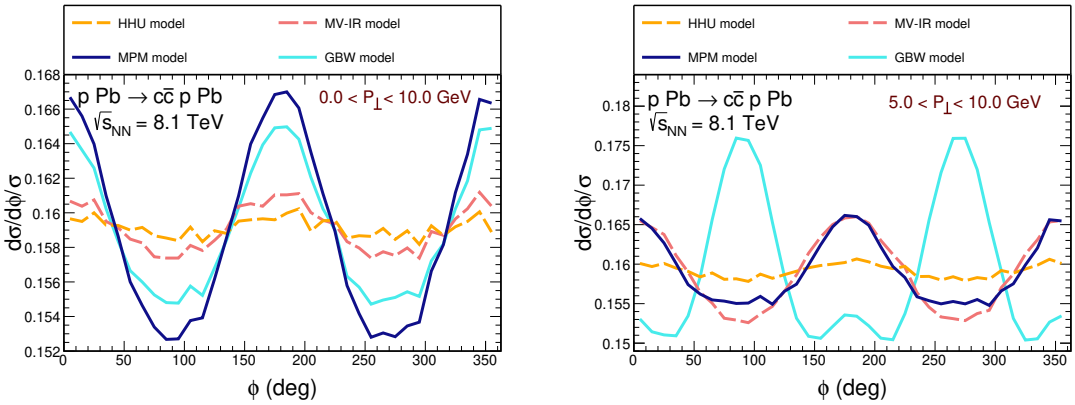

Figure 11. Distributions in the azimuthal angle ϕ between $\vec{P}_\perp$ and $\vec{\Delta}_\perp$ normalised to the total cross section for $0.01 < P_\perp < 10.0\,\text{GeV}$ on the left and for $5.0 < P_\perp < 10.0\,\text{GeV}$ on the right.

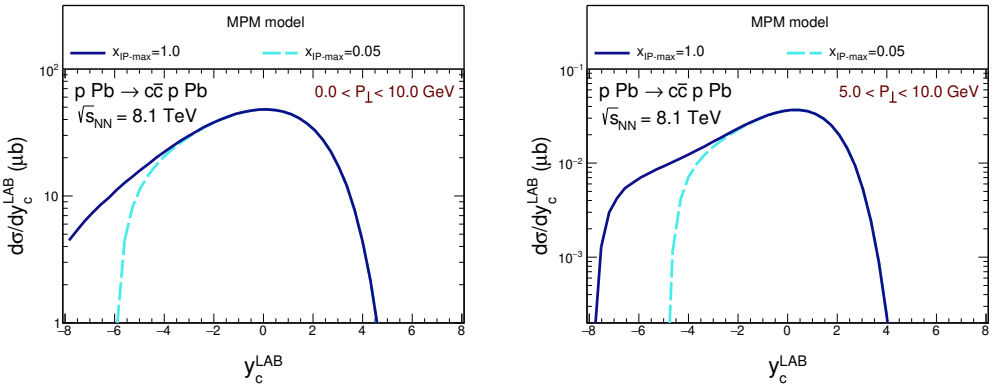

Figure 12. Distributions of MPM model in the y_c^{LAB} for $x_{\mathbb{P}}^{\max} = 1.0$ and $x_{\mathbb{P}}^{\max} = 0.05$.

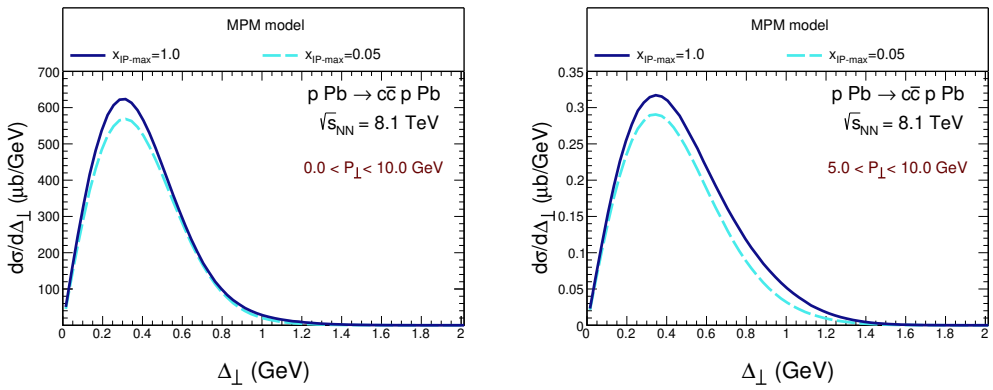

Figure 13. Distributions of MPM model in the $\Delta_\perp$ for $x_{\mathbb{P}}^{\max} = 1.0$ and $x_{\mathbb{P}}^{\max} = 0.05$.

JHEP10(2023)179

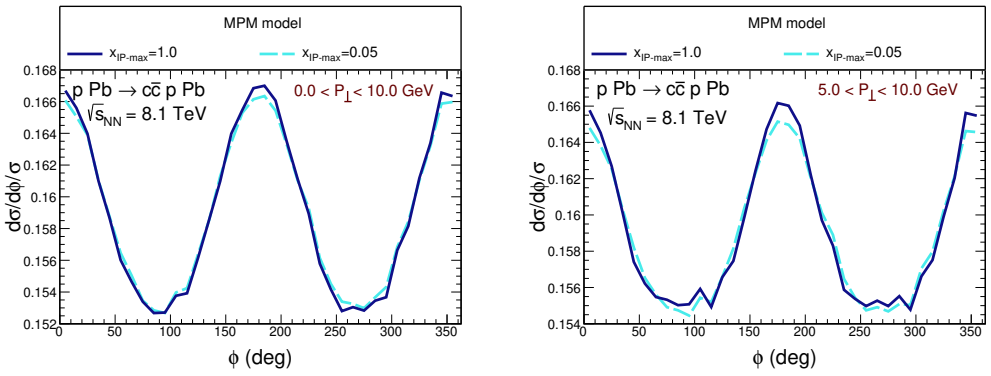

Figure 14. Distributions of MPM model in the azimuthal angle ϕ between $\vec{P}_\perp$ and $\vec{\Delta}_\perp$ normalised to the total cross section for $x_{\mathbb{P}}^{\max} = 1.0$ and $x_{\mathbb{P}}^{\max} = 0.05$.

the LHCb collaboration was able to measure the inclusive $c\bar{c}$ dijets [45] (see also [46]), whether such a measurement would also be possible in the kinematics discussed here is an open issue. The different models give slightly different azimuthal angle distributions. Specially interesting are distributions for $5.0 < P_\perp < 10.0\,\text{GeV}$ where the localization of maxima for some models are reversed.

4 Conclusions

In this paper, we have presented several differential distributions for the diffractive photoproduction of $c\bar{c}$ pairs in the $pA \to p(c\bar{c})A$ reaction at LHC energies. Our results have been obtained using different models for gluon GTMDs from the literature. Some GTMDs were obtained via the Fourier transform of the dipole S-matrix, $N(Y, \vec{r}_\perp, \vec{b}_\perp)$. In this case, the GTMDs are regularized by an extra factor as done already in the literature for exclusive dijet photoproduction. This regularization leads to rather large uncertainties as far as normalization of the cross section is concerned. Therefore, for the distributions derived from dipole amplitudes, one has to focus rather on their shapes than on magnitudes.

In the present work, we go beyond the earlier analysis of ref. [20] considering realistic conditions of proton-lead collisions at the LHC and integrating over the phase space variables (such as quark rapidities and transverse momenta) in the measurable domains. We have paid special attention to azimuthal correlations which were proposed in the literature to test the models of small-x dynamics encoded in the so-called elliptic gluon distributions. We find rather small azimuthal angle modulation in $\phi(\vec{P}_\perp, \vec{\Delta}_\perp)$. The modulations as well as the structure of maxima/minima depends on the GTMD models used in our analysis, so in principle the models can be tested in actual measurements at the LHC. For completeness, we have also presented the predictions for differential distributions in $P_\perp$, $\Delta_\perp$ (transverse momentum of the $c\bar{c}$ pair) and rapidity of the $c\bar{c}$ pair.

Regarding the possible measurement we need to repeat an important caveat. First, for the case of open heavy flavour meson production, a thorough analysis of hadronization corrections would be required to investigate if the sensitivity of our results to the GTMD

JHEP10(2023)179

remains visible at the hadron level. For the case of dijet production, one expects soft gluon emissions (Sudakov resummation) to have an impact, see e.g. ref. [44]. We intend to come back to some of these issues in future work.

Acknowledgments

The authors would like to thank Yoshitaka Hatta for providing grids for numerical solution of the BK equation. This work was partially supported by the Polish National Science Center grant UMO-2018/31/B/ST2/03537 and by the Center for Innovation and Transfer of Natural Sciences and Engineering Knowledge in Rzeszów. R.P. is supported in part by the Swedish Research Council grant, contract number 2016-05996, as well as by the European Research Council (ERC) under the European Union's Horizon 2020 research and innovation programme (grant agreement No. 668679).

A Convolution of amplitude with elliptic GTMD

Here, we collect some steps necessary to analytically perform the azimuthal integration in the convolution of the hard amplitude with the azimuthally asymmetric part of the gluon GTMD. The gluon GTMD is expanded as

$$\begin{aligned} T(Y,\vec{k}_\perp,\vec{\Delta}_\perp) &= T_0(Y,k_\perp,\Delta_\perp) + 2\cos 2(\phi_k-\phi_\Delta)\, T_\epsilon(Y,k_\perp,\Delta_\perp) \\ &= T_0(Y,k_\perp,\Delta_\perp) + 2\,\frac{2(\vec{k}_\perp\cdot\vec{\Delta}_\perp)^2 - k_\perp^2\Delta_\perp^2}{k_\perp^2\Delta_\perp^2}\, T_\epsilon(Y,k_\perp,\Delta_\perp)\,. \end{aligned} \tag{A.1}$$

The parts of the amplitudes that we are interested in, are

$$\begin{aligned} \delta\vec{\mathcal{M}}_0(\vec{P}_\perp,\vec{\Delta}_\perp) &= 2\int\frac{d^2\vec{k}_\perp}{2\pi}\,\frac{\vec{P}_\perp-\vec{k}_\perp}{(\vec{P}_\perp-\vec{k}_\perp)^2+m_Q^2}\,\frac{2(\vec{k}_\perp\cdot\vec{\Delta}_\perp)^2-k_\perp^2\Delta_\perp^2}{k_\perp^2\Delta_\perp^2}\,T_\epsilon(Y,k_\perp,\Delta_\perp) \\ &= 2\left(2\frac{\Delta_\perp^i\Delta_\perp^j}{\Delta_\perp^2}-\delta_{ij}\right)\int\frac{d^2\vec{k}_\perp}{2\pi}\,\frac{\vec{P}_\perp-\vec{k}_\perp}{(\vec{P}_\perp-\vec{k}_\perp)^2+m_Q^2}\,\frac{k_\perp^i k_\perp^j}{k_\perp^2}\,T_\epsilon(Y,k_\perp,\Delta_\perp)\,, \\ \delta\vec{\mathcal{M}}_1(\vec{P}_\perp,\vec{\Delta}_\perp) &= 2\left(2\frac{\Delta_\perp^i\Delta_\perp^j}{\Delta_\perp^2}-\delta_{ij}\right)\int\frac{d^2\vec{k}_\perp}{2\pi}\,\frac{1}{(\vec{P}_\perp-\vec{k}_\perp)^2+m_Q^2}\,\frac{k_\perp^i k_\perp^j}{k_\perp^2}\,T_\epsilon(Y,k_\perp,\Delta_\perp)\,. \end{aligned} \tag{A.2}$$

We now concentrate on the integral over azimuthal angles

$$\vec{I}_{ij} = \int_0^{2\pi}\frac{d\phi_k}{2\pi}\,\frac{\vec{P}_\perp-\vec{k}_\perp}{(\vec{P}_\perp-\vec{k}_\perp)^2+m_Q^2}\,\frac{k_\perp^i k_\perp^j}{k_\perp^2}\,, I_{ij}^1 = \int_0^{2\pi}\frac{d\phi_k}{2\pi}\,\frac{1}{(\vec{P}_\perp-\vec{k}_\perp)^2+m_Q^2}\,\frac{k_\perp^i k_\perp^j}{k_\perp^2}\,. \tag{A.3}$$

This vector integral will be proportional to $\vec{P}_\perp$. We therefore write

$$\vec{I}_{ij} = \frac{\vec{P}_\perp}{P_\perp}\,I_{ij}^0(\vec{P}_\perp,k_\perp)\,, \tag{A.4}$$

with

$$I^0_{ij}(\vec{P}_\perp, k_\perp) = \frac{1}{P_\perp}\int_0^{2\pi}\frac{d\phi_k}{2\pi}\frac{P_\perp^2 - \vec{P}_\perp\cdot\vec{k}_\perp}{(\vec{P}_\perp-\vec{k}_\perp)^2+m_Q^2}\,\frac{k_\perp^i k_\perp^j}{k_\perp^2}\,. \tag{A.5}$$

Now we decompose $I^{0,1}_{ij}$ in terms of invariant functions of $|\vec{P}_\perp|$ and $|\vec{k}_\perp|$ and two orthogonal tensor structures, for which we choose

$$I^{0,1}_{ij}(\vec{P}_\perp) = \left(2\frac{P_\perp^i P_\perp^j}{P_\perp^2} - \delta_{ij}\right)\frac{1}{2}I^{0,1}_\epsilon(P_\perp,k_\perp) + \delta_{ij}\,\frac{1}{2}I^{0,1}_0(P_\perp,k_\perp)\,. \tag{A.6}$$

When inserting this into eq. (A.2), the contraction with δ_{ij} vanishes, an we obtain

$$\begin{aligned}\delta\vec{\mathcal{M}}_0(\vec{P}_\perp,\vec{\Delta}_\perp) &= 2\left(2\frac{(\vec{P}_\perp\cdot\vec{\Delta}_\perp)^2}{P_\perp^2\Delta_\perp^2}-1\right)\frac{\vec{P}_\perp}{P_\perp}\int_0^\infty k_\perp dk_\perp\, I^0_\epsilon(P_\perp,k_\perp)\,T_\epsilon(Y,k_\perp,\Delta_\perp)\\ &= \frac{\vec{P}_\perp}{P_\perp}\,2\cos 2(\phi_\Delta-\phi_P)\int_0^\infty k_\perp dk_\perp\, I^0_\epsilon(P_\perp,k_\perp)\,T_\epsilon(Y,k_\perp,\Delta_\perp)\,.\end{aligned} \tag{A.7}$$

We still need to find the expression for the azimuthal integral $I_\epsilon(P_\perp,k_\perp)$. Introducing

$$a = P_\perp^2 + k_\perp^2 + m^2\,, \qquad b = 2P_\perp k_\perp\,, \tag{A.8}$$

we obtain

$$I^1_\epsilon(P_\perp,k_\perp) = \int_0^{2\pi}\frac{d\phi}{2\pi}\frac{\cos 2\phi}{a-b\cos\phi} \equiv g(a,b)\,, \tag{A.9}$$

and

$$\begin{aligned}P_\perp I^0_\epsilon(P_\perp,k_\perp) &= \int_0^{2\pi}\frac{d\phi}{2\pi}\frac{P_\perp^2-\frac{1}{2}b\cos\phi}{a-b\cos\phi}\,\cos 2\phi\\ &= \int_0^{2\pi}\frac{d\phi}{2\pi}\frac{P_\perp^2-\frac{1}{2}a+\frac{1}{2}(a-b\cos\phi)}{a-b\cos\phi}\,\cos 2\phi\\ &= \left(P_\perp^2-\frac{1}{2}a\right)\int_0^{2\pi}\frac{d\phi}{2\pi}\frac{\cos 2\phi}{a-b\cos\phi}\\ &= \frac{1}{2}(P_\perp^2-k_\perp^2-m^2)g(a,b)\,,\end{aligned} \tag{A.10}$$

where

$$\begin{aligned}g(a,b) &= \frac{1}{b^2}\frac{2a^2-b^2-2a\sqrt{a^2-b^2}}{\sqrt{a^2-b^2}}\\ &= \frac{1}{2P_\perp^2k_\perp^2}\left(\frac{(P_\perp^2+k_\perp^2+m_Q^2)^2-2P_\perp^2k_\perp^2}{\sqrt{(P_\perp^2-k_\perp^2-m_Q^2)^2+4P_\perp^2m_Q^2}}-(P_\perp^2+k_\perp^2+m_Q^2)\right)\,.\end{aligned} \tag{A.11}$$

Here, we used the identity

$$a^2-b^2 = (P_\perp^2+k_\perp^2+m^2)^2-4P_\perp^2k_\perp^2 = (P_\perp^2-k_\perp^2-m^2)^2+4P_\perp^2m^2\,. \tag{A.12}$$

JHEP10(2023)179

References

[1] D. Ashery, *High momentum diffractive processes and hadronic structure*, *Prog. Part. Nucl. Phys.* **56** (2006) 279 [INSPIRE].

[2] N.N. Nikolaev and B.G. Zakharov, *Splitting the pomeron into two jets: A Novel process at HERA*, *Phys. Lett. B* **332** (1994) 177 [hep-ph/9403281] [INSPIRE].

[3] N.N. Nikolaev, W. Schäfer and G. Schwiete, *Coherent production of hard dijets on nuclei in QCD*, *Phys. Rev. D* **63** (2001) 014020 [hep-ph/0009038] [INSPIRE].

[4] X.-D. Ji, *Viewing the proton through 'color' filters*, *Phys. Rev. Lett.* **91** (2003) 062001 [hep-ph/0304037] [INSPIRE].

[5] A.V. Belitsky, X.-D. Ji and F. Yuan, *Quark imaging in the proton via quantum phase space distributions*, *Phys. Rev. D* **69** (2004) 074014 [hep-ph/0307383] [INSPIRE].

[6] S. Meissner, A. Metz and M. Schlegel, *Generalized parton correlation functions for a spin-1/2 hadron*, *JHEP* **08** (2009) 056 [arXiv:0906.5323] [INSPIRE].

[7] C. Lorcé and B. Pasquini, *Structure analysis of the generalized correlator of quark and gluon for a spin-1/2 target*, *JHEP* **09** (2013) 138 [arXiv:1307.4497] [INSPIRE].

[8] R. Boussarie et al., *TMD Handbook*, arXiv:2304.03302 [INSPIRE].

[9] Y. Hagiwara, Y. Hatta and T. Ueda, *Wigner, Husimi, and generalized transverse momentum dependent distributions in the color glass condensate*, *Phys. Rev. D* **94** (2016) 094036 [arXiv:1609.05773] [INSPIRE].

[10] B.Z. Kopeliovich, L.I. Lapidus and A.B. Zamolodchikov, *Dynamics of Color in Hadron Diffraction on Nuclei*, *JETP Lett.* **33** (1981) 595 [INSPIRE].

[11] N.N. Nikolaev and B.G. Zakharov, *Pomeron structure function and diffraction dissociation of virtual photons in perturbative QCD*, *Z. Phys. C* **53** (1992) 331 [INSPIRE].

[12] B.Z. Kopeliovich, H.J. Pirner, A.H. Rezaeian and I. Schmidt, *Azimuthal anisotropy of direct photons*, *Phys. Rev. D* **77** (2008) 034011 [arXiv:0711.3010] [INSPIRE].

[13] E. Iancu and A.H. Rezaeian, *Elliptic flow from color-dipole orientation in pp and pA collisions*, *Phys. Rev. D* **95** (2017) 094003 [arXiv:1702.03943] [INSPIRE].

[14] Y. Hatta, B.-W. Xiao and F. Yuan, *Probing the Small-x Gluon Tomography in Correlated Hard Diffractive Dijet Production in Deep Inelastic Scattering*, *Phys. Rev. Lett.* **116** (2016) 202301 [arXiv:1601.01585] [INSPIRE].

[15] D. Boer and C. Setyadi, *GTMD model predictions for diffractive dijet production at EIC*, *Phys. Rev. D* **104** (2021) 074006 [arXiv:2106.15148] [INSPIRE].

[16] T. Altinoluk, N. Armesto, G. Beuf and A.H. Rezaeian, *Diffractive Dijet Production in Deep Inelastic Scattering and Photon-Hadron Collisions in the Color Glass Condensate*, *Phys. Lett. B* **758** (2016) 373 [arXiv:1511.07452] [INSPIRE].

JHEP10(2023)179

[17] H. Mäntysaari, N. Mueller and B. Schenke, *Diffractive Dijet Production and Wigner Distributions from the Color Glass Condensate*, *Phys. Rev. D* **99** (2019) 074004 [arXiv:1902.05087] [INSPIRE].

[18] F. Salazar and B. Schenke, *Diffractive dijet production in impact parameter dependent saturation models*, *Phys. Rev. D* **100** (2019) 034007 [arXiv:1905.03763] [INSPIRE].

[19] Y. Hagiwara, Y. Hatta, R. Pasechnik, M. Tasevsky and O. Teryaev, *Accessing the gluon Wigner distribution in ultraperipheral pA collisions*, *Phys. Rev. D* **96** (2017) 034009 [arXiv:1706.01765] [INSPIRE].

[20] M. Reinke Pelicer, E. Gräve De Oliveira and R. Pasechnik, *Exclusive heavy quark-pair production in ultraperipheral collisions*, *Phys. Rev. D* **99** (2019) 034016 [arXiv:1811.12888] [INSPIRE].

[21] R. Staszewski, *Forward proton physics at LHC*, in proceedings of the *30th International Workshop on Deep-Inelastic Scattering and Related Subjects (DIS2023)*, East Lansing, MI, U.S.A., 27–31 March 2023, arXiv:2309.02097 [INSPIRE].

[22] ATLAS collaboration, *Prospects for Proton-Proton Measurements with Tagged Protons in ATLAS*, in proceedings of the *International Conference on the Structure and the Interactions of the Photon (Photon 2019)*, Frascati, Italy, 3–7 June 2019, pp. 144–149 [arXiv:1909.10827] [INSPIRE].

[23] CMS and TOTEM collaborations, *The CMS Precision Proton Spectrometer: Precision timing with scCVD diamond crystals*, *Nucl. Instrum. Meth. A* **1047** (2023) 167823 [INSPIRE].

[24] J. Nemchik, N.N. Nikolaev, E. Predazzi, B.G. Zakharov and V.R. Zoller, *The Diffraction cone for exclusive vector meson production in deep inelastic scattering*, *J. Exp. Theor. Phys.* **86** (1998) 1054 [hep-ph/9712469] [INSPIRE].

[25] G. Baur, K. Hencken, D. Trautmann, S. Sadovsky and Y. Kharlov, *Coherent $\gamma\gamma$ and γA interactions in very peripheral collisions at relativistic ion colliders*, *Phys. Rep.* **364** (2002) 359 [hep-ph/0112211] [INSPIRE].

[26] Y.V. Kovchegov and E. Levin, *Quantum Chromodynamics at High Energy*, in *Cambridge Monographs on Particle Physics, Nuclear Physics and Cosmology* **33**, Cambridge University Press (2012) [ISBN: 9780521112574] [DOI:10.1017/9781009291446] [INSPIRE].

[27] V. Barone and E. Predazzi, *High-Energy Particle Diffraction*, in *Texts and Monographs in Physics* **565**, Springer-Verlag, Berlin Heidelberg (2002) [INSPIRE].

[28] N.N. Nikolaev and B.G. Zakharov, *On determination of the large $1/x$ gluon distribution at HERA*, *Phys. Lett. B* **332** (1994) 184 [hep-ph/9403243] [INSPIRE].

[29] N.N. Nikolaev, A.V. Pronyaev and B.G. Zakharov, *Azimuthal asymmetry as a new handle on σ_L/σ_T in diffractive DIS*, *Phys. Rev. D* **59** (1999) 091501 [hep-ph/9812212] [INSPIRE].

[30] I.P. Ivanov, N.N. Nikolaev and A.A. Savin, *Diffractive vector meson production at HERA: From soft to hard QCD*, *Phys. Part. Nucl.* **37** (2006) 1 [hep-ph/0501034] [INSPIRE].

[31] A. Cisek, W. Schäfer and A. Szczurek, *Exclusive production of ρ meson in gamma-proton collisions: $d\sigma/dt$ and the role of helicity flip processes*, *Phys. Lett. B* **836** (2023) 137595 [arXiv:2209.06578] [INSPIRE].

[32] K.J. Golec-Biernat and M. Wüsthoff, *Saturation effects in deep inelastic scattering at low Q^2 and its implications on diffraction*, *Phys. Rev. D* **59** (1998) 014017 [hep-ph/9807513] [INSPIRE].

JHEP10(2023)179

[33] L.S. Moriggi, G.M. Peccini and M.V.T. Machado, *Investigating the inclusive transverse spectra in high-energy pp collisions in the context of geometric scaling framework*, *Phys. Rev. D* **102** (2020) 034016 [arXiv:2005.07760] [INSPIRE].

[34] I. Balitsky, *Operator expansion for high-energy scattering*, *Nucl. Phys. B* **463** (1996) 99 [hep-ph/9509348] [INSPIRE].

[35] Y.V. Kovchegov, *Small-x F_2 structure function of a nucleus including multiple pomeron exchanges*, *Phys. Rev. D* **60** (1999) 034008 [hep-ph/9901281] [INSPIRE].

[36] K.J. Golec-Biernat and A.M. Stasto, *On solutions of the Balitsky-Kovchegov equation with impact parameter*, *Nucl. Phys. B* **668** (2003) 345 [hep-ph/0306279] [INSPIRE].

[37] J. Berger and A. Stasto, *Numerical solution of the nonlinear evolution equation at small x with impact parameter and beyond the LL approximation*, *Phys. Rev. D* **83** (2011) 034015 [arXiv:1010.0671] [INSPIRE].

[38] J. Berger and A.M. Stasto, *Small x nonlinear evolution with impact parameter and the structure function data*, *Phys. Rev. D* **84** (2011) 094022 [arXiv:1106.5740] [INSPIRE].

[39] S.S. Gubser, *Conformal symmetry and the Balitsky-Kovchegov equation*, *Phys. Rev. D* **84** (2011) 085024 [arXiv:1102.4040] [INSPIRE].

[40] L.D. McLerran and R. Venugopalan, *Gluon distribution functions for very large nuclei at small transverse momentum*, *Phys. Rev. D* **49** (1994) 3352 [hep-ph/9311205] [INSPIRE].

[41] H. Kowalski and D. Teaney, *An Impact parameter dipole saturation model*, *Phys. Rev. D* **68** (2003) 114005 [hep-ph/0304189] [INSPIRE].

[42] H. Mäntysaari, K. Roy, F. Salazar and B. Schenke, *Gluon imaging using azimuthal correlations in diffractive scattering at the Electron-Ion Collider*, *Phys. Rev. D* **103** (2021) 094026 [arXiv:2011.02464] [INSPIRE].

[43] V.P. Gonçalves, G. Sampaio dos Santos and C.R. Sena, *Exclusive heavy quark photoproduction in pp, pPb and PbPb collisions at the LHC and FCC energies*, *Nucl. Phys. A* **1000** (2020) 121862 [arXiv:1911.03453] [INSPIRE].

[44] Y. Hatta, B.-W. Xiao, F. Yuan and J. Zhou, *Azimuthal angular asymmetry of soft gluon radiation in jet production*, *Phys. Rev. D* **104** (2021) 054037 [arXiv:2106.05307] [INSPIRE].

[45] LHCb collaboration, *Measurement of differential $b\bar{b}$- and $c\bar{c}$-dijet cross-sections in the forward region of pp collisions at $\sqrt{s} = 13$ TeV*, *JHEP* **02** (2021) 023 [arXiv:2010.09437] [INSPIRE].

[46] R. Maciula and A. Szczurek, *Far-forward production of charm mesons and neutrinos at forward physics facilities at the LHC and the intrinsic charm in the proton*, *Phys. Rev. D* **107** (2023) 034002 [arXiv:2210.08890] [INSPIRE].

JHEP10(2023)179